Potent LILRB1 D1D2-containing antibodies inhibit RIFIN-mediated immune evasions

Yizhuo Wang[1,2,#], Hengfang Tang[1,#], Wanxue Wang[2,3], Ming Li[2], Chenchen Zhu[1,2], Han Dai[1], Hongxin Zhao[1,4,*], Bo Wu[2,*], Junfeng Wang[1,2,*]

[1]High Magnetic Field Laboratory, Key Laboratory of High Magnetic Field and Ion Beam Physical Biology, Hefei Institutes of Physical Science, Chinese Academy of Sciences, Hefei, Anhui 230031, China.

[2]University of Science and Technology of China, Hefei, Anhui 230026, China.

[3]Department of Anatomy, School of Basic Medical Sciences, Anhui Medical University, Hefei, China.

[4]Hefei China Science Longwood Biological Technology Co., Ltd. Hefei, Anhui 230088, China.

[#] Those authors contributed equally.

*Corresponding authors. Email: zhx@hmfl.ac.cn (Hongxin Zhao), wubo@hmfl.ac.cn (Bo Wu), junfeng@hmfl.ac.cn (Junfeng Wang).

Abstract

Variant surface antigens of *Plasmodium falciparum*, including RIFIN, play a pivotal role in malaria pathogenesis and facilitate immune evasion by binding to immunoinhibitory receptors such as LILRB1. Recently, receptor-containing antibodies have been discovered in malaria-exposed individuals and uncover a novel antibody mechanism in inhibiting immune evasions of *Plasmodium falciparum*. Previous studies have identified several LAIR1- and LILRB1 D3D4-containing antibodies. However, no antibodies containing LILRB1-D1D2 have been identified, even though some RIFINs interact with LILRB1-D1D2. In this study, we propose a in vitro strategy for the generation of this type of antibodies by employing structure-based affinity maturation. Using this strategy, we successfully generated D1D2.v-IgG, an antibody that effectively blocks the specific binding of RIFIN#1 (from PF3D7_1254800) to LILRB1. Furthermore, we developed NK-biAb, a bispecific antibody targeting RIFIN#1 and the NKG2D receptor based on D1D2.v-IgG. Both antibodies demonstrate promising results in augmenting NK cell-mediated cytotoxicity against RIFIN#1-expressing K562 cells, with NK-biAb exhibiting superior efficacy. The present strategy could be generally used for developing antibodies against the malarial parasite-host interactions, thereby facilitating advancements in malaria treatments and vaccines.

Keywords: *Plasmodium falciparum*, immune evasion, RIFIN, receptor-containing antibody

43 **Introduction**

44 Malaria is one of the most deadly infectious diseases that affect human health,
45 leading to nearly half a million deaths annually. The disease is caused by infection with
46 *Plasmodium parasites*, with *Plasmodium falciparum* (*P. falciparum*) being the most
47 lethal species[1,2]. The emergence and dissemination of drug-resistant parasites threaten
48 malaria control and elimination globally and raise the demand for new malaria
49 treatments and vaccines[3-5].

50 The life cycle of *P. falciparum* is complex, consisting of multiple developmental
51 stages from the mosquito vector to the human host. Among them, the blood stage is
52 responsible for the clinical symptoms of malaria[6,7]. During this stage, *P. falciparum*
53 invades erythrocytes and replicates within them, while also expressing a number of
54 variable surface antigens on infected erythrocytes (IEs). Blood-stage parasites are the
55 main target of acquired immunity. However, *P. falciparum* employs multiple strategies
56 to evade immune responses by interacting with host receptors through variable surface
57 antigens, which is believed to contribute to the slow development of naturally acquired
58 immunity against malaria. PfEMP1 and RIFIN are two of the three major multigene
59 familiy proteins expressed on the surface of IEs. PfEMP1 proteins have been found to
60 interact with various human endothelial receptors to mediate the adhesion of the IEs to
61 the surfaces of blood vessels and tissues, thus facilitating *P. falciparum* to escape
62 splenic clearance. RIFINs comprise the largest family of variable surface antigens
63 in *P. falciparum*[7,8]. Some RIFINs have been shown to mediate immune suppression by
64 binding to and activating inhibitory immune receptors on myeloid and lymphoid cells ,
65 such as leukocyte-associated immunoglobulin-like receptor 1 (LAIR1) and leukocyte
66 immunoglobulin-like receptor B1 (LILRB1)[9-12] (Fig. 1a). In theory, blocking those
67 surface antigen-receptor interactions, thereby preventing the immune escape of malaria
68 parasites maybe a promising strategy to develop effective malaria treatments and
69 vaccines[13,14]. Notably, the recent identification of the LAIR1- and LILRB1-containing
70 antibodies in malaria-exposed individuals suggests that the human immune system

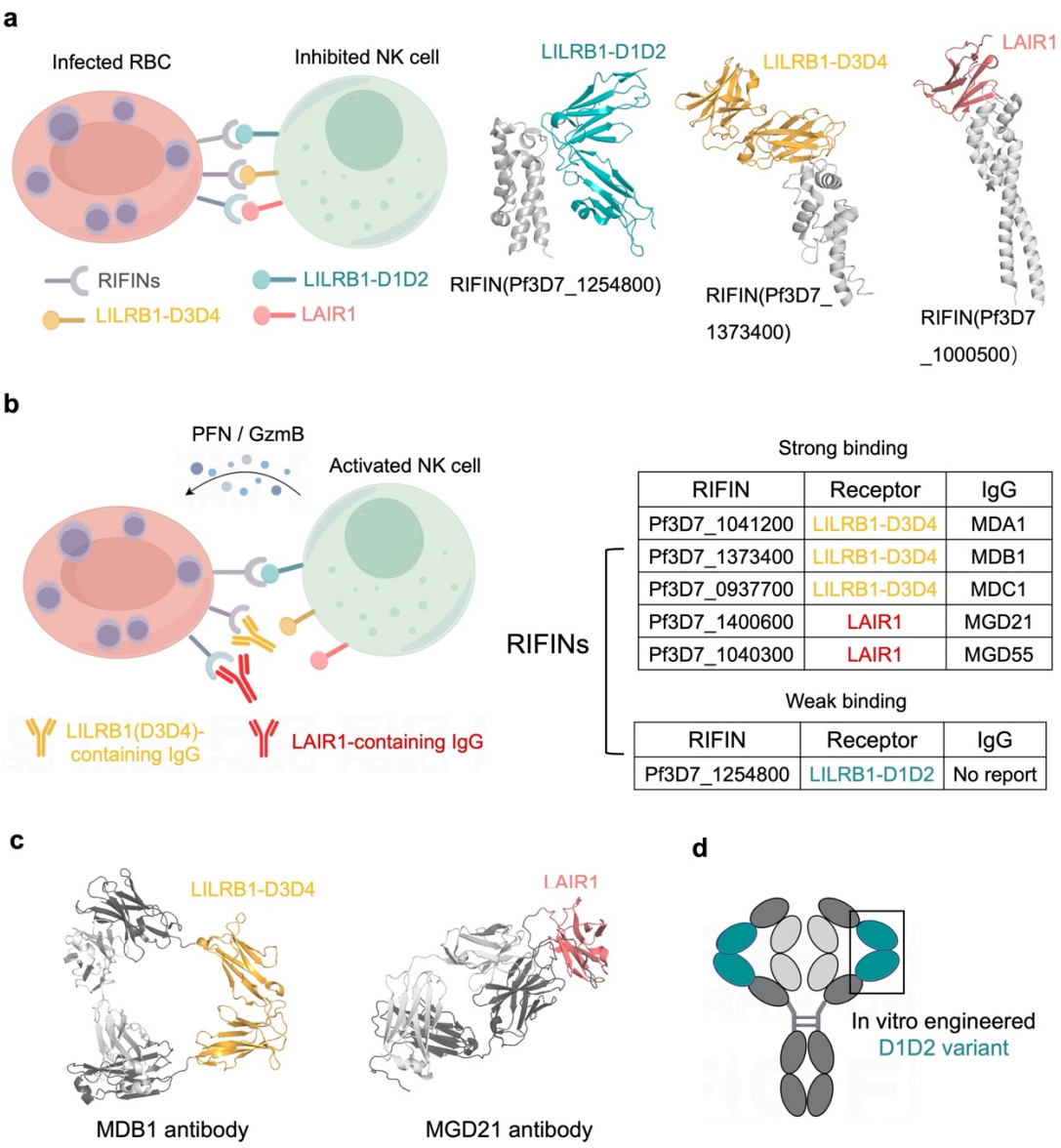

Figure 1. Immune evasion of *P.falciparum* and design of novel receptor-containing antibody

(**a**) The mechanism of immune evasion of *P. falciparum* and structures of RIFIN and immunoinhibitory receptors**.** Different RIFIN subtypes bind to their corresponding receptor domains to transduce immunoinhibitory signals (PDB: 6ZDX, 7KFK and 7F9N). (**b**) Receptor-containing antibodies in inhibiting immune evasion of *P. falciparum* and identification of LILRB1- and LAIR1-containing antibodies. All reported LILRB1-containing antibodies only have LILRB1-D3D4 domains and no antibodies that contain LILRB1-D1D2 domains were found. (**c**) Two representative receptor-containing antibody. The left one is LILRB1 D3D4-containing antibody MDB1 (PDB:7KHF) and the right one is LAIR1-containing antibody MGD21 (PDB: 7JZ4). (**d**) Strategy for generating high-affinity LILRB1 D1D2-containing antibodies. Affinity-matured

82 LILRB1-D1D2 variant is generated through in vitro structure-based affinity maturation and then the
83 LILRB1-D1D2 variant is grafted into the framework of MDB1 by replacing LILRB1-D3D4
84 domains.
85
86 employs this strategy to combat immune evasions of malaria parasites[15-17] (Fig. 1b).
87 LAIR1-containing antibodies reveal specific mutations inside LAIR1 inserts, resulting
88 in high affinity toward RIFINs[16]. Different from LAIR1-containing antibodies,
89 LILRB1-containing antibodies reveal no mutation in LILRB1 inserts and all LILRB1
90 inserts are LILRB1-D3D4 domains or just LILRB1-D3 domain within the variable-
91 constant (VH-CH1) elbow region[15] (Fig. 1c). Antibodies that contain LILRB1-D1D2
92 domain have not been identified, which might be due to the low affinity between RIFIN
93 and LILRB1-D1D2. Moreover the in vivo formation of receptor-containing antibody is
94 time-consuming; in particular, the maturation sites of the receptor-containing antibody
95 during in vivo affinity-maturation are uncontrollable.
96 Here, we propose a strategy for the design of novel receptor-containing antibodies.
97 Our strategy features obtaining a high-affinity receptor fragment variant through in
98 vitro structure-based affinity maturation[18-20] and then the affinity-matured receptor
99 fragment variant is grafted into the framework of a human natural antibody MDB1[15]
100 against malaria by replacing LILRB1-D3D4 domains in MDB1 (Figure 1d). Using this
101 strategy, a novel LILRB1 D1D2-containing antibody, D1D2.v-IgG, was successfully
102 generated. The binding affinity of D1D2.v-IgG to RIFIN is about 110-fold higher than
103 that of LILRB1. Biochemical and cellular assays have demonstrated that this antibody
104 can effectively block the RIFIN#1-LILRB1 interaction, and significantly augment the
105 NK cell-mediated cytotoxicity against RIFIN#1-expressing K562 cells. Furthermore,
106 based on the D1D2.v-IgG, a bi-specific antibody NK-biAb was engineered by
107 incorporating the natural killer group 2 D (NKG2D) receptor-specific scFv KYK2.0[21-
108 23] at its C-terminus, mimicking CAR-NK therapy[24,25]. It is worth noting that this bi-
109 specific antibody exhibits an enhanced capacity to augment NK cell-mediated

110 cytotoxicity compared to D1D2.v-IgG. Our work provides a novel antibody design
111 approach targeting the interaction between malaria parasite variant surface antigens and
112 host receptors, which could be useful for development malaria treatments and vaccines.

113

114 **Results**

115 **Structure-guided engineering of a high affinity LILRB1 D1D2 variant**

116 RIFIN#1, via its variable region binds to the extracellular domain (ECD) of
117 LILRB1 with a moderate affinity (K_d =570 ± 130 nM). LILRB1-ECD comprises four
118 immunoglobulin-like domains (D1-D4), and its complex structure with RIFIN#1
119 demonstrates that the interaction is mediated by the D1D2 domain[9]. In order to obtain
120 a high-affinity agent capable of competitively antagonizing LILRB1-RIFIN#1
121 interaction, we carried out a structure-guided directed evolution of the LILRB1-D1D2
122 domain by yeast surface display. The LILRB1-RIFIN#1 complex structure was used as
123 a guide for designing LILRB1 D1D2 mutation library. As shown in Fig. 2a, based on
124 the structural information, ten LILRB1 D1D2 residues in the interface with RIFIN#1
125 (K42, E68, G97, A98, Y99, I100, Q125, V126, F128, E184) were varied by random
126 PCR. The resulting D1D2 mutation library contained 2×10^7 transformants. The library
127 was then displayed on the yeast surface and stained by biotinylated RIFIN and subjected
128 to selections in order to isolate high-affinity binders (Fig. 2b and Fig. S1). A total of
129 eight rounds of sorting were conducted (Fig. S2). Following three rounds of sorting
130 with decreasing concentrations of biotinylated RIFIN tetramers (2 μM, 1 μM and 0.3
131 μM) (Fig. S3) and three rounds of sorting with decreasing concentrations of biotinylated
132 RIFIN monomers (0.3 μM, 0.1μM and 0.02 μM) (Fig. S4), two rounds of kinetic
133 competition sorting were performed using 0.02 μM biotinylated RIFIN monomers in
134 the presence of approximately a 50-fold excess unlabeled competition RIFIN, with a
135 duration of 2 h and 4 h respectively (Fig. S5). After completing all eight rounds of
136 sorting, yeast cells were plated to obtain single clones. DNA sequencing shows that a

single D1D2 mutant clone (named D1D2.v) dominates this enrichment process, and this consensus variant contains 9 total mutations: K42M, G97S, A98T, Y99F, I100T, Q125E, V126I, F128Q, E184H (Fig. 2c and Fig. S6).

To gain insight into the mechanisms underlying affinity enhancement in D1D2.v, we utilized SWISS-MODEL to obtain a structural model of D1D2.v binding to RIFIN#1 (Fig. 2d). A comparative analysis with the crystal structure of LILRB1-RIFIN#1 complex suggested that D1D2.v bound to RIFIN#1 in a manner essentially identical with its wild-type counterpart; however, some distinctions were observed at the binding interface. As shown in Fig. 2d, the Q125E mutation establishes a new salt bridge with R233 on RIFIN#1. In addition, it appears that the G97S, A98T and I100T mutations enhance their H-bonding strength towards RIFIN#1 based on analysis of H-bonding distances.

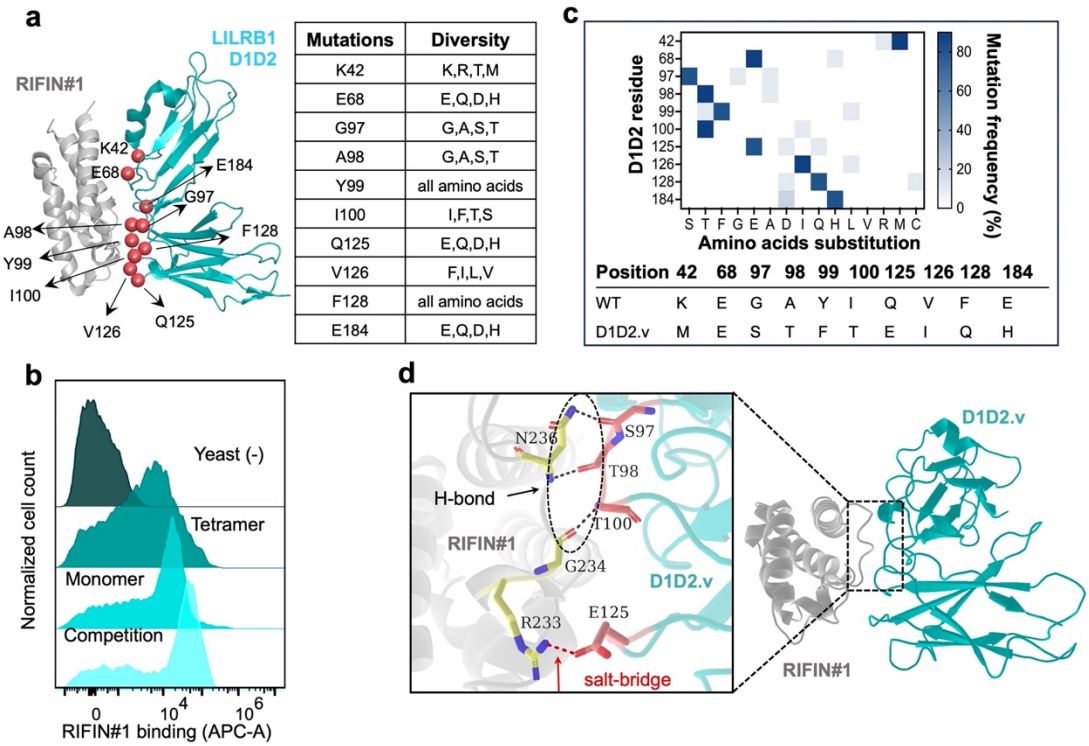

Mutations	Diversity
K42	K,R,T,M
E68	E,Q,D,H
G97	G,A,S,T
A98	G,A,S,T
Y99	all amino acids
I100	I,F,T,S
Q125	E,Q,D,H
V126	F,I,L,V
F128	all amino acids
E184	E,Q,D,H

Figure 2. Yeast display and affinity maturation of D1D2 domain

(**a**) (Left) LILRB1 models based on LILRB1-RIFIN#1 complex structure (PDB:6ZDX), where RIFIN#1 is in orange color, LILRB1-D1D2 is in cyan color, and the randomized positions are depicted by red balls; (Right) tabulated randomized positions of the LILRB1-D1D2 interface library

with possible amino acid variants. (**b**) Flow cytometry results for the yeast stained with biotinylated RIFIN#1 in tetramer, monomer and competition selection methods. (**c**) The frequency of mutations (Above) and consensus D1D2.v sequence (Below). (**d**) Structural modeling and interface analysis. The sequences of D1D2.v and RIFIN#1 were imported into the SWISS-MODEL server for initial model generation based on the coordinates of PDB code**.** G97S, A98T, I100T and Q125E mutations in D1D2.v increases H-bonding strength targeting RIFIN#1, while a salt-bridge forms between E125 on D1D2.v and R233 on RIFIN#1.

Design and biochemical characterization of a D1D2.v-containing antibody that antagonizes RIFIN#1-LILRB1 interaction.

Recently, several natural LILRB1-containing monoclonal antibodies have been discovered in individuals exposed to malaria, such as MDB1, wherein the LILRB1 D3D4 domain is inserted within its variable-constant (VH-CH1) elbow region[15,16]. We then generated a D1D2.v-containing antibody, named D1D2.v-IgG, by substituting the LILRB1-D3D4 insertion in MDB1 with D1D2.v (Fig. 3a). For expression as a secreted protein, the codon-optimized antibody sequence was genetically linked to a N-terminal Trp2 signal peptide sequence within a pTT5 expression vector. The recombinant antibody was transiently expressed in Expi293F cells and purified from culture supernatant by protein A affinity chromatography. The purity was confirmed by SDS-PAGE analysis under both non-reducing and reducing conditions. To assess the RIFIN#1-binding activity of this recombinant antibody, we initially generated the Fab fragment by enzymatically removing the Fc tag and test its binding with RIFIN#1 by size-exclusion chromatography (SEC) assay. The results indicate a robust binding between the Fab and RIFIN#1, forming a tight complex (Fig. 3b). Next, we quantified the binding affinity of D1D2.v-IgG to RIFIN#1 using a protein-based ELISA assay, employing the purified LILRB1 ECD as a control. As shown in Fig. 3c, the dissociation constant (K_d) for the binding of LILRB1 ECD to RIFIN#1 is approximately 650 nM,

182 which is consistent with the previously reported affinity determined using surface
183 plasmon resonance (SPR). In stark contrast, D1D2.v-IgG exhibits a significantly higher
184 affinity towards RIFIN#1, with a K_d of 6 nM representing a 110-fold improvement (Fig.
185 3c). To assess the ability of D1D2.v-IgG to antagonize LILRB1 binding to RIFIN#1,
186 we conducted a competitive ELISA assay. The results revealed that this antibody
187 effectively inhibited LILRB1 binding to RIFIN#1 in a dose-dependent manner with a
188 half-maximal inhibitory concentration (IC50) of 20 nM (Fig. 3d).

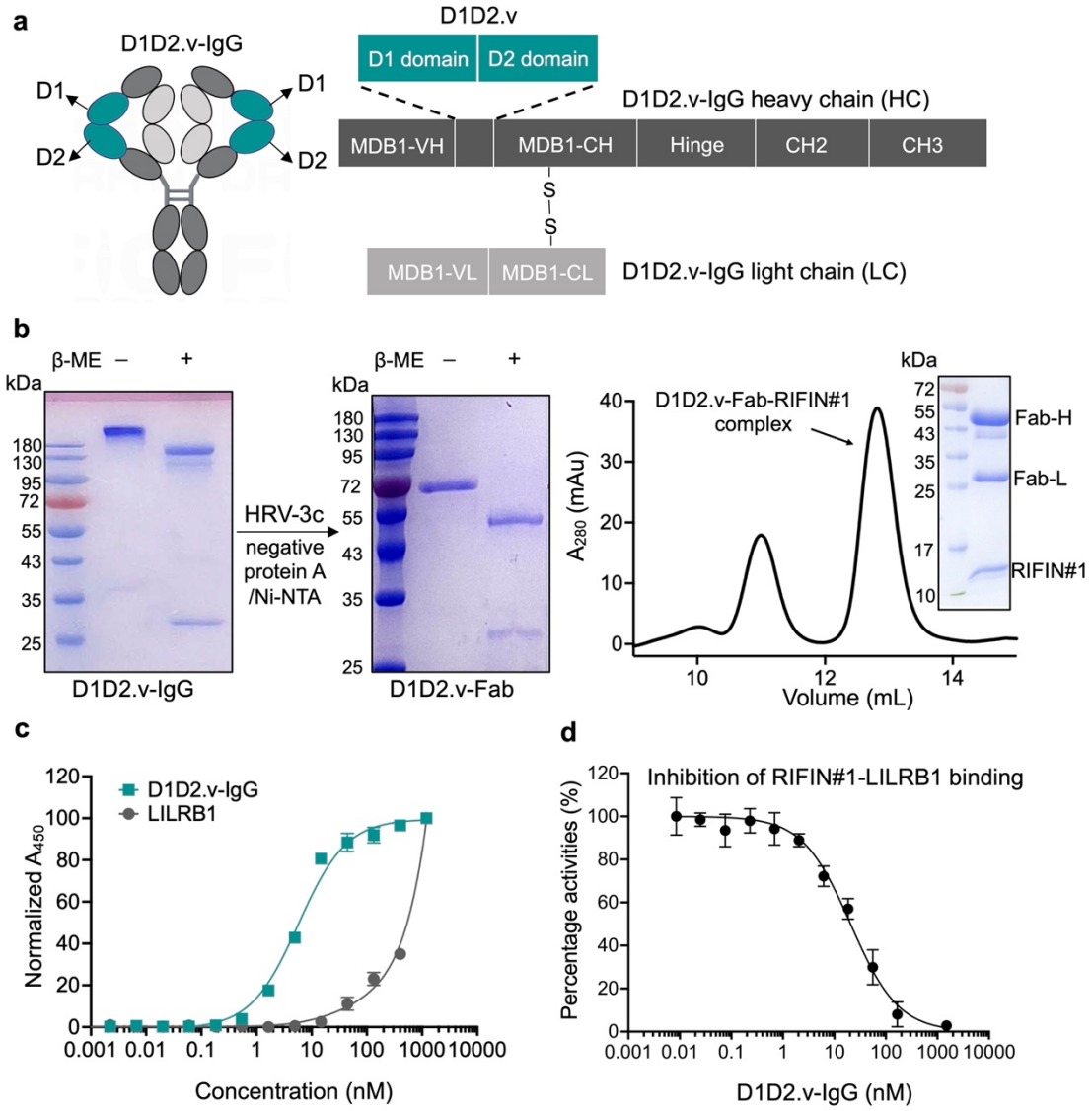

189

190 **Fig.3: Molecular design and biochemical characterization of the D1D2 (V)-IgG**

191 **(a)** Molecular structure and cDNA frame of D1D2 domain containing IgG. Inserted LILRB1-D1
192 domain was colored in dark blue and LILRB1-D2 domain was colored in light blue, which were

193 located between heavy variable chain (VH) and heavy constant chain (CH). Antibody heavy chain
194 and Fc domain were depicted in dark grey and light chain was depicted in light grey. (**b)** Purification
195 and functional validation of the antigen binding fragment (Fab) of D1D2.v-IgG. SDS-PAGE (Left)
196 show the purity and molecular weight of D1D2.v-IgG before protease digestion. SDS-PAGE (Right)
197 show the purity and molecular weight of D1D2.v-Fab. Size-exclusion chromatography (SEC)
198 chromatograms show the homogeneous Fab-RIFIN complex have a UV_{280} absorbance at around 13
199 mL. **(c)** Titration curves of wild-type LILRB1 (ECD) (dark green) and D1D2.v-IgG (red) binding
200 to RIFIN in ELISA assay. Data are mean ± SD. (**d)** The representative competition binding curve
201 using wild type LILRB1 (ECD) showed D1D2.v-IgG antagonized the RIFIN-LILRB1 (ECD)
202 interaction effectively. Data represent mean ± SD of three technical replicates.
203
204
205 **D1D2.v-IgG significantly enhances NK92 cytolytic activity against RIFIN#1-**
206 **expressing K562 cells in vitro**
207 Given that the binding of RIFIN#1 to LILRB1 leads to the suppression of NK cell
208 response, we subsequently investigated whether D1D2.v-IgG could enhance NK cell-
209 mediated cytotoxicity by blocking the interaction between LILRB1 and RIFIN#1. To
210 assess this, we conducted NK92 cell cytotoxicity assays on K562 cells stably
211 transfected with full length RIFIN#1 (Fig. S7). The expression level of LILRB1on
212 NK92 cells was validated by flow cytometry (Fig. 4a). The RIFIN#1-expressing K562
213 cells were co-cultured with NK92 cells at two different effector to target (E:T) ratios of
214 2.5 and 12.5 in the presence or absence of D1D2.v-IgG. Flow cytometry analysis
215 confirmed the specific binding of purified D1D2.v-IgG to the RIFIN#1-expresssing
216 K562 cells (Fig. 4b). At an E:T ratio of 2.5, the observed cytotoxicity against RIFIN#1-
217 expresssing K562 cells was 5.8% in the absence of D1D2.v-IgG, which significantly
218 increased to 13.8% upon addition of D1D2.v-IgG at concentrations of 100 nM.
219 Similarly, at an E:T ratio of 12.5, the cell killing efficiency was 35% in the absence of
220 D1D2.v-IgG, but remarkably rose to 61% when treated with D1D2.v-IgG at

concentrations of 100 nM (Fig. 4c). Moreover, we observed that D1D2.v-IgG significantly augmented the secretion of perforin and granzyme B from NK92 cells (Fig. 3d-e). These findings clearly demonstrate that D1D2.v-IgG can effectively stimulate NK-cell cytotoxicity against RIFIN#1-expressing K562 cells.

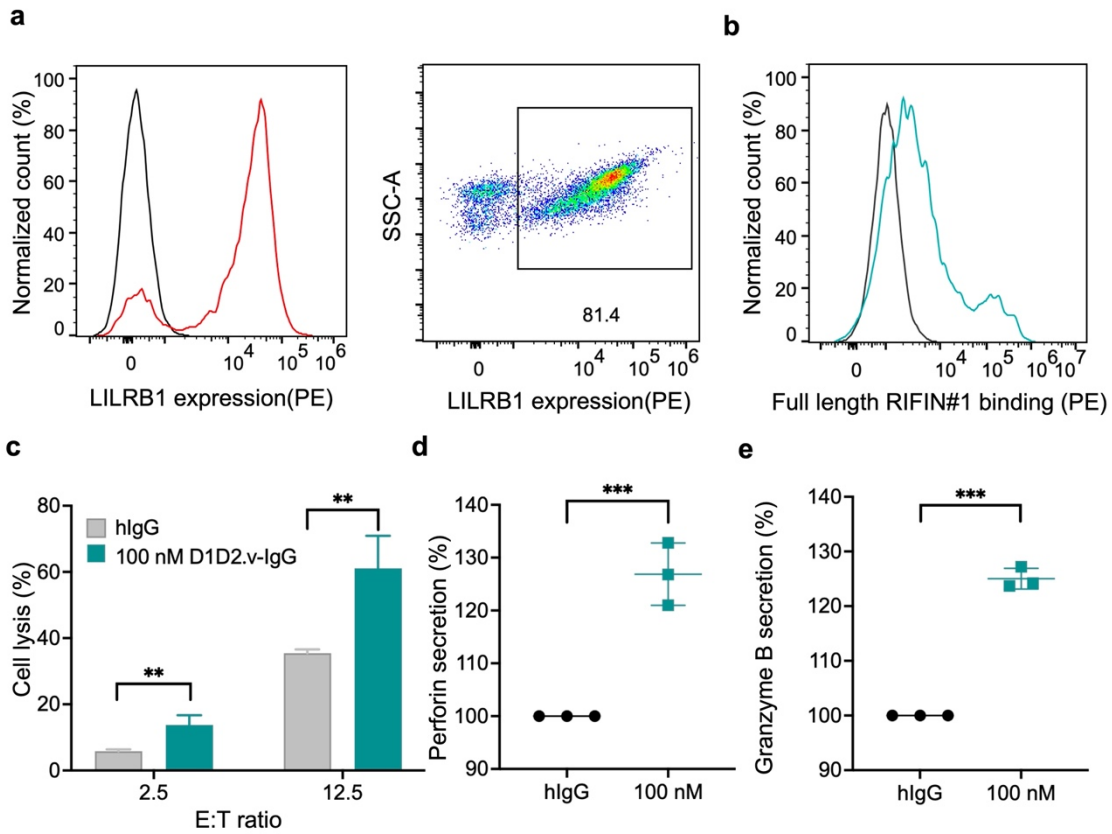

Fig.4: D1D2.v-IgG enhanced NK cell cytotoxicity against RIFIN-expressing K562 cell

(**a**) Detection of the LILRB1 on NK92 cells by flow cytometry. The red curve shows the binding of LILRB1 antibody to LILRB1 on NK92 cells, while the blue curve informs the control sample of NK92 cells. (**b**) Detection of the purified D1D2.v-IgG bound to RIFIN#1-expressing K562 cells by flow cytometry. The red curve shows the binding of D1D2.v-IgG to full-length RIFIN#1 on stably-transfected K562 cells, while the cyan curve informs the blank sample of K562 cells. **(c)** The results for the NK92 cytotoxicity in the presence or absence of D1D2.v-IgG. RIFIN#1-expressing K562 cells were cocultured with NK92 cells and incubated with 100 nM control human IgG (hIgG) (Grey, n = 3) or 100 nM D1D2.v-IgG (Yellow, n = 3). (**d,e**) Detections of the perforin (e) and granzyme B (f) releases in the presence or absence of D1D2.v-IgG. RIFIN#1-expressing K562 cells were cocultured with NK92 cells (E: T ratio = 1: 1) and incubated with 100 nM control hIgG (Grey, n =

237 3) or 100 nM D1D2.v-IgG (Orange, n = 3). After the incubation for 24h, the perforin and granzyme
238 B levels were determined by ELISA. Statistical test was t test and statistical significance was
239 analyzed between D1D2.v-IgG and hIgG. *P<0.05; **P<0.01; ***P<0.001; ****P<0.0001.
240
241
242 **Generation of a bispecific antibody targeting RIFIN#1 and NKG2D**
243 Next, we aim to develop a bispecific antibody capable of recruiting NK cells to
244 RIFIN#1-expressing cells using the D1D2.v-IgG as a basis. The redirection of NK cells
245 necessitates a highly specific and high-affinity 'compass' (Fig. 5a). To fulfill this
246 requirement, we have chosen an engineered scFv known as KYK2.0, which exhibits a
247 nanomolar affinity towards NKG2D expressed on all types of NK cells. By fusing the
248 scFv form of KYK2.0 to the C terminal of the Fc fragment of D1D2.v-IgG through a
249 flexible GS linker, we have generated a bispecific antibody (bsAb), named NK-biAb
250 (Fig. 5b). The resulting bsAb was then transiently expressed and purified from
251 Expi293F cell culture supernatants via affinity chromatography. Integrity and purity of
252 NK-biAb were analyzed by SDS-PAGE under reducing and non-reducing conditions
253 (Fig. S8a). As anticipated, this purified bispecific antibody demonstrated the ability to
254 bind to both NK cells and RIFIN#1-expressing K562 cells in flow cytometry analysis
255 (Fig. S8b-c).
256

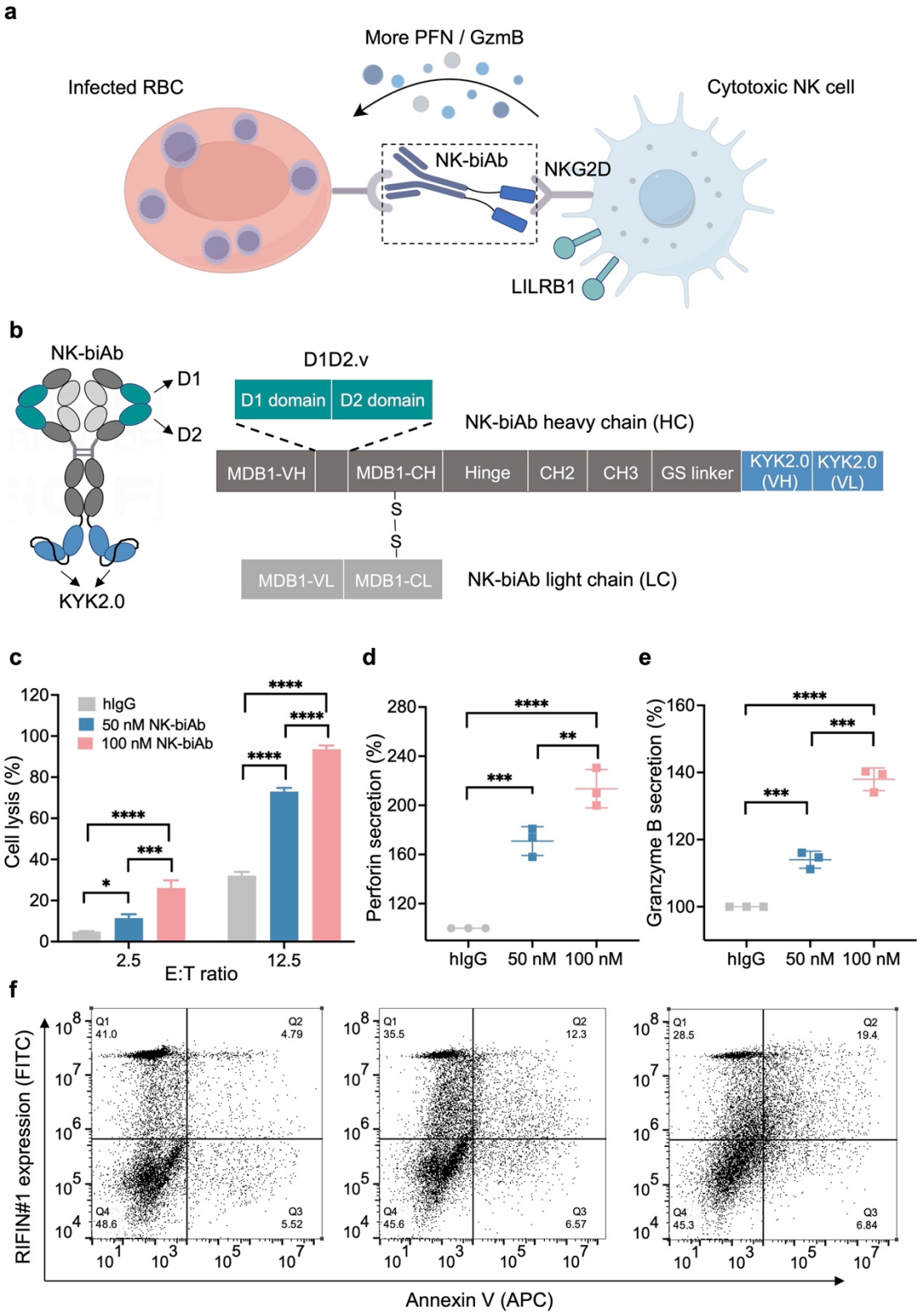

Fig.5: Design and characterization of NK-biAb

(a) Schematic of NK cell redirections by NK-biAb. Scfv form of KYK2.0 (scfv-KYK2.0), an NKG2D activating antibody was fused to C terminus of D1D2.v-IgG. When recognizing and blocking immune escape response of *P. falciparum* via D1D2.v-Fab domains, scfv-KYK2.0 domain

262 can also bind to NKG2D receptors, redirect NK cells to *P. falciparum* and trigger NK cell activities.
263 scFv-KYK2.0 was colored in light orange and NKG2D receptor was depicted as a light blue dart.
264 **(b)** cDNA frame of NK-biAb. cDNA of D1D2.v-IgG part is the same as previously described. The
265 heavy variable chain (VH) and light variable chain (VL) of KYK2.0 depicted in orange are fused to
266 C terminus of D1D2.v-IgG by a GS linker. (**c)** NK92 cytotoxicity assay in the presence of NK-biAb.
267 RIFIN#1-expressing K562 cells were cocultured with NK92 cells and incubated with 100 nM
268 control human IgG (hIgG) or 50 nM NK-biAb (Cyan, n =3) and 100 nM NK-biAb (Red, n =3).
269 Statistical tests were two-way ANOVA and statistical significance was analyzed between NK-biAb
270 and hIgG. **(d,e)** Detections of the perforin (d) and granzyme B (e) releases in the presence or absence
271 of NK-biAb. RIFIN#1-expressing K562 cells were cocultured with NK92 cells (E: T ratio = 1: 1)
272 and incubated with 100 nM control hIgG (Grey, n = 3), 50 nM NK-biAb (Cyan, n =3) and 100 nM
273 NK-biAb (Red, n = 3). After the incubation for 24h, the perforin and granzyme B levels were
274 determined by ELISA. Statistical tests were one-way ANOVA and statistical significance was
275 analyzed between NK-biAb and hIgG. **(f)** Flow detection results for the coculture of NK92 and
276 RIFIN#1-expressing K562 for 24 h at E: T = 1: 1 in the presence of 100 nM hIgG (Left), 50 nM
277 NK-biAb (Middle) and 100 nM NK-biAb (Right), showing the RIFIN#1-expressing K562 cells
278 killed by NK92 cells. The data in the second quadrant stands for the lysed RIFIN#1-expressing
279 K562 cells. *P<0.05; **P<0.01; ***P<0.001; ****P<0.0001.
280
281
282 **NK-biAb exhibits an enhanced ability to trigger NK92 cytotoxicity against**
283 **RIFIN#1-expressing K562 cells.**
284 Finally, we evaluated the impact of NK-biAb on NK cell cytotoxicity against
285 RIFIN#1-expressing K562 cells. As shown in figure, this bispecific antibody exhibited
286 a significantly enhanced ability to trigger NK cytotoxicity compared to the
287 monospecific antibody D1D2.v-IgG. When treatment with a concentration of 100 nM
288 NK-biAb, there was a remarkable enhancement in cytotoxic efficiency from 13.8% to
289 26.1% and from 61%-93.6%, again at E/T ratios of 2.5 and 12.5 respectively, compared

290 to treatment with D1D2.v-IgG under identical conditions (Fig. 5c). In the presence of
291 50 nM and 100 nM NK-biAb, NK92 cells secreted more perforin and granzyme B
292 compared to treatment with D1D2.v-IgG (Fig. 5d-5e). Flow cytometry results also
293 validated that NK-biAb can potently stimulate NK-cell cytotoxicity against RIFIN#1-
294 expressing K562 cells (Fig. 5f).
295
296
297 **Discussion**
298 Upon infection, *P. falciparum* employs variant surface antigens to engage with
299 receptors on the human host, thereby facilitating immune evasion and ensuring their
300 survival within the host organism[7,8]. Recent investigations have identified several
301 receptor-containing antibodies in individuals exposed to malaria that possess the
302 capability to impede surface antigen-receptor interactions. Functional studies have
303 demonstrated that these antibodies hold potential as therapeutic agents and for
304 incorporation into malaria vaccine design[15-17]. For instance, MGD21 antibody has been
305 shown to promote NK cell-dependent lysis of IEs and inhibit *P. falciparum* growth[17].
306 In this study, we propose a in vitro strategy for the design of novel receptor-
307 containing antibodies. Our approach utilizes structure-guided affinity maturation to
308 obtain a receptor fragment variant with enhanced binding capability, while leveraging
309 the framework of a human natural antibody against malaria as a template for generating
310 an antibody[15]. Due to the weak affinity between RIFIN and LILRB1-D1D2, no related
311 D1D2-containing antibody has been reported. We used this strategy to artificially create
312 high-affinity D1D2-containing antibodies that fill a gap in this field. As an illustrative
313 example, we have successfully generated D1D2.v-IgG, an antibody that exhibits a 110-
314 fold higher affinity towards RIFIN1# than LILRB1 and is capable of effectively
315 blocking the interaction between RIFIN1# and LILRB1. Cellular assays demonstrated
316 that this antibody significantly enhances NK cell-mediated cytotoxicity against K562
317 cells expressing RIFIN#1. Furthermore, based on D1D2.v-IgG, we have developed a

318 bispecific antibody that targets both RIFIN#1 and the NKG2D receptor, which
319 demonstrates superior ability to enhance NK cell-mediated cytotoxicity compared to
320 D1D2.v-IgG. Bispecific antibodies have been shown to be a promising avenue for
321 immunotherapeutic interventions against diverse malignancies[21,22,24,26]. Our data
322 underscore the potential application of these agents in combating malaria.

323 In summary, our study provides a strategy for designing receptor-containing
324 antibodies, offering potential applications in the development of malaria therapeutics
325 and vaccines. The increasing availability of resolved structures of Plasmodium surface
326 antigens binding to host receptors[9,11,15,17] will facilitates the development of
327 corresponding antibodies using our strategy.

328

329 **Materials and Methods**

330 **Antigen purifications**

331 The variable region of RIFIN#1 (PF3D7_1254800, 165-274 aa) with an N-
332 terminal 6×His tag was cloned into a pET28a vector. The recombinant vector was
333 transformed into E.coli BL21 (gold), and the cells were induced with 1 mM IPTG at a
334 OD_{600} of 0.7. Protein was expressed as inclusion bodies and denatured in a guanidine
335 buffer (6 M Guanidine hydrochloride, 20 mM Tris pH 8.0, and 300 mM NaCl) for 4 h.
336 The inclusion bodies were then purified by Ni-NTA affinity chromatography and eluted
337 by the guanidine buffer containing additional 500 mM imidazole. The denatured
338 inclusion bodied were retrieved by dialyzing against a buffer (20 mM Tris pH 8.0, 300
339 mM NaCl) and resolubilized in the guanidine buffer. Refolding was performed by the
340 quick dilution of inclusion bodies into a buffer (1 M L-arginine, 20 mM Tris pH 8.5,
341 100 mM NaH_2PO_4, 2 mM ethylenediaminetetraacetic acid, 0.1 mM
342 phenylmethylsulfonyl fluoride, 3 mM reduced glutathione and 0.3 mM oxidized
343 glutathione) until a final protein concentration of 0.1 mg/mL-0.2 mg/mL. The refold
344 RIFIN#1 was further polished on a Superdex 75 Increase column in a PBS (pH 7.2)
345 buffer. The ECD of human LILRB1 gene with a C-terminus His tag was cloned into a

346 pTT5 vector, and the vector was then PEI-transfected into Expi293F cells (Procell,
347 China). After a post-transfection for 96 h, the supernatant was collected and the protein
348 was purified with a Ni-NTA affinity chromatography. The purified LILRB1-ECD was
349 further exchanged into PBS (pH 7.2) buffer on a Superdex 200 Increase column.
350 For biotinylation, the RIFIN#1 and LILRB1-ECD proteins were cultured with
351 NHS-pEG12-biotin in a PBS buffer (pH 7.2). The culture reactions were quenched with
352 a Tris buffer after 8 h incubation. The free NHS-pEG12-biotin reagents were splitted
353 from the biotin-labeled proteins by a size-exclusion chromatography.
354
355 **EBY100 vector construction and LILRB1-D1D2 wild type display**
356 To avoid weird display stuff, pYD1 vector was reconstructed by fusing Agar 1/2
357 domain to the C-terminus of displayed targets. Meanwhile, the detection tags of pYD1
358 vector were replaced by a N-terminal FLAG, a C-terminal V5-tag and a C-terminal His
359 tag. D1D2 wild type was co-electroporated with a precut reconstructed pYD1, while
360 yeast cells were induced with SGCAA. The signals of RIFIN#1 binding to the displayed
361 D1D2 wild type were detected by FCM.
362
363 **Constructing the library of D1D2 variants**
364 Based on the crystal structure of RIFIN#1-LILRB1 complex, a site-directed
365 library was generated by the several rounds of overlapping PCR reactions for
366 randomizing the binding residues of LILRB1-D1D2. The randomizing primers are as
367 shown in Supplementary Table 1.The overlapping PCR reactions were conducted under
368 20 cycles. The external primers for the amplification of LILRB1-D1D2 library on a
369 large scale introduce a 70 bp homologous sequence to pYD1 vector. The LILRB1-
370 D1D2 library were co-transformed into EBY100 with a precut pYD1 vector at a
371 library/vector ratio of 3: 1. Yeast transformants were recovered in a YPD/Sorbitol broth
372 and amplified in SDCAA, resulting in a library containing 2×10^7 transformants.
373

374 **MACS selections of the naive library**

375 Transformed yeast were induced in SGCAA medium at 20°C for 48 h. For the 1st
376 round selection, 4×10^8 cells referred to as 20× library size were pellet and washed with
377 a PBE buffer (PBS pH 7.2 supplemented with 0.5% BSA). Firstly, the cells were
378 resuspended in 2 mL of the PBE buffer containing 2 μM biotinylated RIFIN that had
379 been pre-coated with Streptavidin-Alexa Fluor 647 (Invitrogen, USA), followed by an
380 incubation at 4°C for 2 h. Secondly, the stained cells were pelleted by centrifugation
381 (3500 g, 5 min) , washed twice with 2 mL PBE, and resuspended in PBE containing
382 paramagnetic anti-Alexa Fluor 647 microbeads (Miltenyi Biotech, German). Thirdly, a
383 magnetically-labeled yeast cells were enriched on LS MACS column (Miltenyi Biotech,
384 German), and the enriched yeast cells were eluted with 5-10 mL PBE. Finally, the
385 selection outputs were pellet and amplified in SDCAA for next round selection. Five
386 additional selections were performed by successively decreasing concentrations of
387 biotinylated RIFIN#1 from 1 μM to 0.02 μM. In each round selection, the yeast cells
388 were first labeled with SAV-Alexa Fluor 647 after incubating with biotinylated
389 RIFIN#1 for 2 h and washed once with PBE, then coated with 100 μL of anti-Alexa
390 Fluor 647 microbeads for 30 min and washed once, and finally separated by LS MACS
391 column.

392

393 **MACS competition selections**

394 The MACS tetramer/monomer selection outputs were further performed
395 competition selections to get ultrahigh affinity variants. The induced tetramer/monomer
396 selection outputs were cultured with 0.02 μM biotinylated RIFIN#1 at 4°C for 2 h. Then
397 the cells were pellet, washed once with PBE and competed with 1 μM unlabeled
398 RIFIN#1 for 2 h. After the competition process, the cells were stained with
399 Streptavidin-Alexa Fluor 647 and coated with anti-Alexa Fluor 647 microbeads. MACS
400 sorting was also performed using LS column. By now, the 1st round competition was
401 finished, and the competition outputs were amplified and induced for next round

402 competition selection. In the 2nd round competition selection, the competing time of
403 unlabeled RIFIN was increased to 4 h, and the final selection outputs were titrated on
404 SDCAA plates for plasmid extraction and sequencing.
405
406 **Preparation of D1D2.v-IgG**
407 D1D2.v were inserted between MDB1-VH and MDB1-CH, and cloned into pTT5
408 vector as IgG4 forms. MDB1 light chain was also cloned to pTT5 vector. The DNAs
409 of MDB1 light chains and D1D2.v-IgG heavy chains were co-transfected into
410 Expi293F cells using PEI transfection reagents. After the transfection for 96 h, the
411 culture supernatant was separated by centrifugation (4000 rpm, 10 min) and purified
412 with protein A resin. The purified D1D2.v-IgG was further polished on a Superdex 200
413 Increase column in a PBS (pH 7.4) buffer.
414
415 **Characterization of D1D2.v-IgG**
416 Protein-based ELISA assays were performed to determine the affinity of D1D2.v-
417 IgG to RIFIN#1 in comparison to that of LILRB1-ECD. First, RIFIN#1 (5 μg/mL) was
418 immobilized on 96-well ELISA plates and incubated with D1D2.v-IgG of different
419 concentrations. Then, the plates were washed with PBST for 3 times and cultured with
420 the anti-human IgG-HRP at 1: 5000 dilution. Finally, the wells were washed with PBST,
421 developed with TMB for 15 min, and quenched with 2 M HCl. The absorbance at 450
422 nm was determined by a microplate reader.
423 For the protein-competition ELISA assay, RIFIN#1 (5 μg/mL) was immobilized
424 on 96-well ELISA plates, and cocultured with D1D2.v-IgG of different concentrations
425 and a competing biotinylated LILRB1 (ECD) of 1-1.5× K_d concentration, where K_d is
426 the dissociation constant. Then the plates were washed with PBST for 3 times and
427 cultured with HRP-conjugated streptavidin at 1: 2000 dilution. The absorbance at 450
428 nm was recorded by a microplate reader.
429

430 **Purifying Fab fragment of D1D2.v-IgG and its functional validation**

431 D1D2.v-IgG was digested by His-tagged HRV-3c protease overnight and
432 subjected to a negative protein A and Ni-NTA column purification. The 5-fold excess
433 of refold RIFIN#1 were co-cultured with the Fab fragment of D1D2.v-IgG and the
434 resulting complex was further polished on a Superdex 200 Increase column. The ratio
435 of RIFIN#1 binding to the Fab fragment of D1D2.v-IgG was assessed by SDS-PAGE.

436

437 **Preparation of NK-biAb and its functional validation**

438 scFv-KYK2.0 was fused to the C-terminus of D1D2.v-IgG heavy chain to generate
439 NK-biAb (M_r = 260 kDa). The DNAs of MDB1 light chains and NK-biAb heavy chains
440 were co-transfected into Expi293F cells using PEI transfection reagents. After the
441 transfection for 96 h, the culture supernatant was collected by centrifugation (4000 rpm,
442 10 min) and purified on a protein A column. The purified protein was further polished
443 on a Superdex 200 Increase column in a PBS (pH 7.4) buffer. To validate the functions
444 of NK-biAb to attach NK92 cells and bind NKG2D, the NK92 cells pre-stimulated with
445 IL-2 were cultured with NK-biAb at 37°C for 2 h, and stained with anti-human IgG-PE
446 for the detection of surface NKG2D.

447

448 **Stable RIFIN#1-expressing K562 cell line production**

449 K562 cells (Procell, China) were cultured at 37°C in DMEM with 10% FBS and
450 5% CO_2. The cDNA of RIFIN#1 with its natural signal peptide was cloned into pLVX-
451 ZsGreen plasmid. Lentivirus were produced by HEK-293T (Procell, China) for
452 infecting K562 cells. The infected K562 cells were enriched by the selection using 1
453 μg/mL puromycin, to obtain the stable RIFIN#1-expressing K562 cell line.

454

455 **Evaluation of NK cell cytotoxicity**

456 The RIFIN#1-expressing K562 cells were incubated at 37°C for 1 h with D1D2.v-
457 IgG or NK-biAb. The NK92 cells in the same volume as RIFIN#1-expressing K562

458 cells were then cocultured for 4 h at 37°C and 5% CO_2 with the incubated RIFIN#1-
459 expressing K562 cells at the E: T ratios of 2.5: 1 and 12.5: 1. The final mixtures contain
460 either 100 nM D1D2.v-IgG or 50 nM/100 nM NK-biAb. The killing efficiency (E) was
461 calculated from the absorbance (A) of CCK8 at 450 nm: $E\% = [1-(A_S-A_{EC})/A_{TC}]\times 100\%$,
462 where A_S is for the mixture of effector and target cells, and A_{EC} and A_{TC} are, respectively,
463 for effector cells and target cells.
464
465 **Cytokine measurement and FCM detection**
466 10^5 NK92 cells were cocultured for 24 h with 10^5 RIFIN#1-expressing K562 cells
467 in a 96-well plate in the presence of either 100 nM D1D2.v-IgG or 50 nM/100 nM NK-
468 biAb. Perforin and granzyme B release were detected from the supernatants of the
469 cocultured mixture by protein-based ELISA assay kits (Beyotime, China). The mixtures
470 of NK92 and K562-RIFIN#1 cells were stained for 1 h at ca. 4ºC (controlled by ice)
471 with Annexin V-APC in 100 μL PBS containing 0.5% BSA. The stained cells were
472 detected by flow cytometry, with the data analyzed by Flowjo software.
473
474
475
476 **Reference**
477 1. Organization., W. H. World Malaria Report *World Malaria Report* (2016).
478 2. Burton, D. R. Antibodies, viruses and vaccines. *Nature Reviews Immunology* **2**, 706-
479 713 (2002).
480 3. Haldar, K., Bhattacharjee, S. & Safeukui, I. Drug resistance in *Plasmodium*. *Nature*
481 *Reviews Microbiology* **16**, 156-170 (2018).
482 4. Burton, D. R. What Are the Most Powerful Immunogen Design Vaccine Strategies?
483 Reverse Vaccinology 2.0 Shows Great Promise. *Cold Spring Harb Perspect Biol*
484 **9**(2017).

485 5. Wells, T. & Donini, C. Monoclonal Antibodies for Malaria. *New England Journal of*
486 *Medicine* **387**, 462-465 (2022).
487 6. Nilsson, S. K., Childs, L. M., Buckee, C. & Marti, M. Targeting Human Transmission
488 Biology for Malaria Elimination. *PLOS Pathogens* **11**, e1004871(2015).
489 7. Sakoguchi, A. & Arase, H. Mechanisms for Host Immune Evasion Mediated by
490 *Plasmodium falciparum*-Infected Erythrocyte Surface Antigens. *Frontiers in*
491 *Immunology* **13** (2022).
492 8. Chan, J. A., Fowkes, F. J. & Beeson, J. G. Surface antigens of *Plasmodium*
493 *falciparum*-infected erythrocytes as immune targets and malaria vaccine candidates.
494 *Cell Mol Life Sci* **71**, 3633-3657(2014).
495 9. Harrison, T. E. *et al.* Structural basis for RIFIN-mediated activation of LILRB1 in
496 malaria. *Nature* **587**, 309-312 (2020).
497 10. Saito, F. *et al.* Immune evasion of *Plasmodium falciparum* by RIFIN via inhibitory
498 receptors. *Nature* **552**, 101-105 (2017).
499 11. Xie, Y. *et al.* Structural basis of malarial parasite RIFIN-mediated immune escape
500 against LAIR1. *Cell Rep* **36**, 109600 (2021).
501 12. Willcox, B. E., Thomas, L. M. & Bjorkman, P. J. Crystal structure of HLA-A2
502 bound to LIR-1, a host and viral major histocompatibility complex receptor. *Nature*
503 *Immunology* **4**, 913-919 (2003).
504 13. Wahl, I. & Wardemann, H. How to induce protective humoral immunity against
505 *Plasmodium falciparum* circumsporozoite protein. *Journal of Experimental Medicine*
506 **219** (2022).
507 14. Cockburn, I. A. & Seder, R. A. Malaria prevention: from immunological concepts
508 to effective vaccines and protective antibodies. *Nature Immunology* **19**, 1199-1211,
509 doi:10.1038/s41590-018-0228-6 (2018).
510 15. Chen, Y. *et al.* Structural basis of malaria RIFIN binding by LILRB1-containing
511 antibodies. *Nature* **592**, 639-643 (2021).

512 16. Tan, J. *et al.* A LAIR1 insertion generates broadly reactive antibodies against
513 malaria variant antigens. *Nature* **529**, 105-109 (2016).
514 17. Xu, K. *et al.* Structural basis of LAIR1 targeting by polymorphic *Plasmodium*
515 RIFINs. *Nature Communications* **12**, 4226 (2021).
516 18. Chao, G. *et al.* Isolating and engineering human antibodies using yeast surface
517 display. *Nature Protocols* **1**, 755-768(2006).
518 19. Weiskopf, K. *et al.* Engineered SIRPα variants as immunotherapeutic adjuvants to
519 anticancer antibodies. *Science* **341**, 88-91(2013).
520 20. Gonzalez-Perez, D. *et al.* Affinity-matured DLL4 ligands as broad-spectrum
521 modulators of Notch signaling. *Nature Chemical Biology* **19**, 9-17(2023).
522 21. Kwong, K. Y., Baskar, S., Zhang, H., Mackall, C. L. & Rader, C. Generation,
523 affinity maturation, and characterization of a human anti-human NKG2D monoclonal
524 antibody with dual antagonistic and agonistic activity. *J Mol Biol* **384**, 1143-
525 1156(2008).
526 22. Zhang, C. *et al.* Bispecific antibody-mediated redirection of NKG2D-CAR natural
527 killer cells facilitates dual targeting and enhances antitumor activity. *J Immunother*
528 *Cancer* **9** (2021).
529 23. Zhao, C. *et al.* A new approach to produce IgG (4)-like bispecific antibodies. *Sci*
530 *Rep* **11**, 18630 (2021).
531 24. Wolf, N. K., Kissiov, D. U. & Raulet, D. H. Roles of natural killer cells in immunity
532 to cancer, and applications to immunotherapy. *Nature Reviews Immunology* **23**, 90-105
533 (2023).
534 25. Albinger, N., Hartmann, J. & Ullrich, E. Current status and perspective of CAR-T
535 and CAR-NK cell therapy trials in Germany. *Gene Therapy* **28**, 513-527 (2021).
536 26. Leaver-Fay, A. *et al.* Computationally Designed Bispecific Antibodies using
537 Negative State Repertoires. *Structure* **24**, 641-651 (2016).
538

Acknowledgements: Funding was provided by the National Key R&D Program of China (Grant No. 2023YFA1607500), the National Natural Science Foundation of China (Grant No. 32371362), and the Anhui Major Basic Research Projects (Grant No. 2023z04020016).

Author contributions: Y.W and H.T contributed equally to this work. Y.W initiated the project, performed the library construction and selections, prepared antigen samples and performed biochemical assays. H.T performed the FCM detections and conducted the stable cell line production, cytotoxicity assays and ELISA assays. W.W performed the antibody purifications and functional validations. L.M helped to prepare biotinylated sample preparations. C.Z helped to perform biochemical assays and FCM detections. Y.W. and B.W analyzed the data, interpreted the results. J.W, H.D and B.W prepared the manuscript. J.W., B.W and H.Z supervised the project. All authors read and edited the manuscript.

Competing interests: The authors declare no competing interests.

Data and materials availability: All data and materials are available within the paper and its supplementary materials. Extra data are available from the corresponding author (J. Wang) upon reasonable request.

List of Supplementary Materials

Fig S1 to S8 for multiple supplementary figures

Table S1 for supplementary table